Chemical Engineering Journal 150 (2009) 447–454

Contents lists available at ScienceDirect

Chemical Engineering Journal

journal homepage: www.elsevier.com/locate/cej

Tuning the cycle length in the NO_x storage-reduction process and its contribution to the real-flow scenario

U. Elizundia, R. López-Fonseca*, M.A. Gutiérrez-Ortiz, J.R. González-Velasco

Chemical Technologies for Environmental Sustainability Group, Department of Chemical Engineering, Faculty of Science and Technology, Universidad del País Vasco/EHU, P.O. Box 644, E-48080 Bilbao, Spain

ARTICLE INFO

Article history:
Received 30 September 2008
Received in revised form 15 December 2008
Accepted 19 January 2009

Keywords:
Lean-burn engines
NO_x storage-reduction catalyst
$Pt/Ba/Al_2O_3$
Ideal-real flow
Mixing effects

ABSTRACT

The influence of reductant supply timing on the performance of a $Ba/Pt–Al_2O_3$ model storage-reduction catalyst was analysed. This study was developed in terms of NO_x and CO conversion, CO availability for NO_x ad-species reduction and temperature profile analysis. A relevant $CO–O_2$ mixing effect was noticed during lean-to-rich and rich-to-lean transitions. On the basis of constant overall amount of reductant, the intensity of this effect was dependent on the number of transitions per time unit. Then, an excessive cycle length reduction led to operation states with CO defect, that subsequently controlled NO_x conversion and temperature profiles over the catalyst. This mixing effect was related to the deviation from ideal plug flow condition. In this real-flow context, and due to the inherently transient NSR operation, the need for a quantitative description of those departures from idealised flow was evidenced. A first approach, just for the case of a discrete lean-to-rich transition, was presented in this work.

1. Introduction

Diesel and lean-burn gasoline engines reduce the fuel consumption of vehicles and the related CO_2 emissions with respect to stoichiometric gasoline engines. These kinds of engines, together with low tailpipe emissions in order to meet emission standards for NO_x, CO, hydrocarbons and particulate matter (PM), merge as an important advance in the name of the efficient and environmentally friendly use of the energy resources [1].

However, the high oxygen content in the exhaust gas reduces the activity of three way catalysts for NO_x reduction and inhibits the achievement of the required emission levels [2]. In this O_2 rich environment and as an alternative to a single catalytic step reduction process (selective catalytic reduction and catalytic decomposition of NO_x), NO_x storage and reduction catalysts (NSR) have claimed to be a potential tool for effective nitrogen oxides abatement [2–5]. This technique is based on the use of a catalyst, which has a high surface area carrier where a noble metal and an alkaline metal oxide are dispersed, with the $Pt–Ba/Al_2O_3$ system the most common formulation studied in the literature [6–10]. Cyclical NSR operation involves the storage of NO_x on alkaline oxide adsorption sites during lean-burn operation. The periodic transition to shorter rich periods, when stored NO_x are released, allows the regeneration of the trapping ability. Subsequently, NO_x is reduced to N_2 over the noble metal component in this net reducing atmosphere [4,11].

This transient environment, with cyclical transitions to rich conditions, over the NSR catalyst can be imposed by the engine air-to-fuel (A/F) ratio control system (typically of spark-ignited vehicles). Current diesel engines offer certain flexibility on A/F ratio [12] but fuel injection, which could be processed over an upstream reformer [5], has been typically used in these vehicles. For the spark-ignited engine case, the reductant (CO was selected in this study) may participate in a series of parallel reactions during the rich periods, which are included in Eq. (1). On one hand, the presence of CO is necessary for the gas-phase reduction of NO_x (reactions ii–iii). Further, during these rich excursions, enough CO must be present in order to complete the process for the regeneration and reduction of adsorbed NO_x (reactions iv–v), which can appear as nitrites and/or nitrates [8]. For the sake of simplicity in these reactions BaO was supposed to be formed in these reactions. However, in the presence of CO_2 and H_2O the formation of $BaCO_3$ or $Ba(OH)_2$ along with BaO is expected as well [9]. Moreover, CO will be also involved in consuming the remaining oxygen either in the gas phase (from incomplete combustion on the cylinders or due to gas mixing effects during those cyclical transitions) and on the catalyst surface ("oxygen storage capacity") (OSC), reaction i [13]. Reaction vi, H_2 formation from CO via water-gas-shift reaction, should not be neglected as well as

* Corresponding author. Tel.: +34 94 6015985; fax: +34 94 6015963.
E-mail address: ruben.lopez@ehu.es (R. López-Fonseca).

1385-8947/$ – see front matter © 2009 Elsevier B.V. All rights reserved.
doi:10.1016/j.cej.2009.01.044

its subsequent contribution to the detailed reactions i–v [14].

$$\begin{aligned}
&\text{i.} && CO + (1/2)O_2 \rightarrow CO_2 \\
&\text{ii.} && 2CO + 2NO \rightarrow N_2 + 2CO_2 \\
&\text{iii.} && 4CO + 2NO_2 \rightarrow N_2 + 4CO_2 \\
&\text{iv.} && 5CO + Ba(NO_3)_2 \rightarrow 5CO_2 + N_2 + BaO \\
&\text{v.} && 3CO + Ba(NO_2)_2 \rightarrow 3CO_2 + N_2 + BaO \\
&\text{vi} && CO + H_2O \rightleftharpoons CO_2 + H_2
\end{aligned} \quad (1)$$

The viability of the NSR catalytic technology is determined by catalyst costs as well as fuel consumption concerns. Therefore, in order to limit the fuel economy loses, the length of the rich spikes should be limited in lean-burn gasoline engines [15]. Several studies have been focused on maximising regeneration efficiency since this would result in improving fuel economy. The effects of the chemical nature of the reductant and the catalyst design have already been studied [16–20]. The effects of dynamic NSR behaviour under transient conditions have been addressed as well [21–26]. Epling et al. [22] showed the competition between NO_x and oxygen storage compounds for the reductant, quantifying the contribution of the later for their catalyst. In a following study [23], they analysed the impact of concomitant exothermic events due to the reductant-stored O_2 reaction on the storage phase. On the other hand, Muncrief et al. [24] indicated that, for transitions simulating fuel injection, very long or very short cycle durations do not exploit the operational benefits of lean/rich cycling. This dependence of a powder catalyst on cycle timing was also valid for a monolithic NSR converter [25]. Less attention has been paid to quantifying the contribution of reductant-gas-phase O_2 reaction and its influence on the process efficiency. It could be expected that this reaction's main effect would be related to the decrease in the reductant availability for the regeneration of adsorption sites and the subsequent NO_x reduction, but it also may contribute to both NO_x release due to the released heat of reaction and the NO_x storage process due to the slow dissipation of this released heat [23,26].

In this context, the main objective of the present work was to analyse and quantify the extent of the reaction of CO with O_2 together with the subsequent exothermic events as a function of cycle timing. We also focused on NSR catalyst performance not only in terms of NO_x conversion, but also analysing the degree of the CO slip and the CO availability for NO_x ad-species reduction. The study was developed for a simple model $Pt/Ba/Al_2O_3$ catalyst (powder) without any specific OSC component capable of masking $CO–O_2$ mixing effects. The experimental set-up was designed to mimic engine controlled lean-to-rich and rich-to-lean transitions. Moreover, O_2 was not admitted during the rich periods. This experimental operational mode is expected to only enable the occurrence and extent of this $CO–O_2$ reaction owing to mixing effects during these transitions.

2. Experimental

2.1. Catalyst preparation and characterisation

The model $Ba/Pt–Al_2O_3$ catalyst used in this study was prepared through wetness impregnation on a γ-Al_2O_3 (Axens) carrier. $Pt(NH_3)_4(NO_3)_2$ (Alfa Aesar) and $Ba(CH_3COO)_2$ (Aldrich Chemical Co.) were used as the precursors for Pt and BaO, respectively. The γ-Al_2O_3, previously sized (0.3–0.5 mm) and calcined at 700 °C, was dipped consecutively into Pt and Ba solutions. The slurry obtained after each immersion was dried in a rotary device at 30 °C and 3 mmHg and subsequently calcined at 550 °C for 4 h.

The $Pt(0.8)/Ba(12.8)/Al_2O_3$ composition was established using a PerkinElmer Aanalyst 100 atomic absorption spectrometer. BET (Brunauer, Emmett, and Teller) surface areas of 140 and 84 $m^2\ g^{-1}$ were measured for Al_2O_3 and $Pt/BaO/Al_2O_3$ samples, respectively, in a Micromeritics ASAP2000 equipment. A reduction in Pt dispersion, determined by H_2 chemisorption at 30 °C using the aforementioned experimental device, from 21 to 5% was caused by Ba incorporation.

2.2. Reactor configuration and NSR tests

Catalytic runs were performed in a vertical downward flow stainless steel reactor with a 13 mm inner diameter. All the

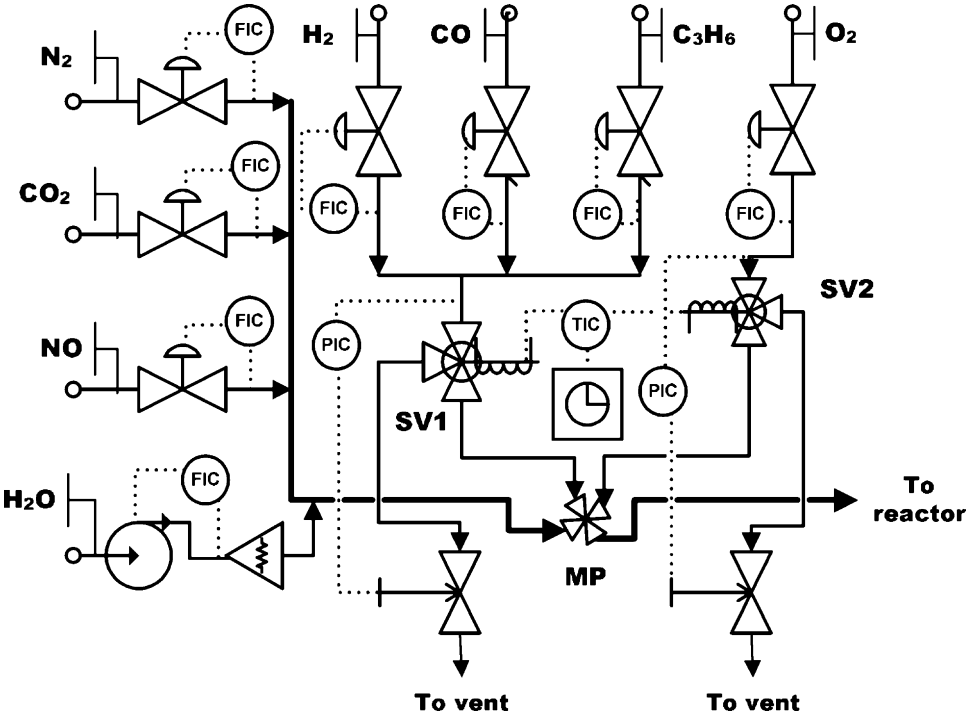

Fig. 1. Experimental set-up for the catalytic runs.

Table 1
Nominal gas compositions for lean and rich periods.

	NO, ppm	CO, %	O_2, %	H_2O, %	CO_2, %
Lean conditions	900	–	5.0	8.0	8.0
Rich conditions	945	2.0	–	8.4	8.4

experiments were conducted at a space velocity of 60,000 h^{-1}, corresponding to a bed height of 3 cm (bed volume of 4 cm^3) and a gas flow rate of 4 N l min^{-1}. Simulated exhaust gases were fed through an attached manifold system (Fig. 1), which allowed precision mixture of N_2, O_2, H_2O, CO, CO_2, H_2 and NO. Each gas was fed via calibrated mass flow controllers and N_2 was used as the balance gas. Controlled H_2O vapour flow was also incorporated into the stream by means of a heated conduction. The resulting gas-phase nominal compositions are listed in Table 1.

CO was selected as the only reductant compound admitted during the rich events. During the rich period O_2 flow was not maintained so as to simulate a spark engine system in which transitions are due to changes in engine operation. In order to prevent O_2 and CO mixing, both streams were delivered to a common mix point (MP) with the main stream. The use of two solenoid valves (SV1 and SV2) in those streams allowed precise definition of the lean and rich time periods (t_L and t_R, respectively). The path between MP and SV1 and SV2 was minimised so as to avoid significant dead volume areas. Thus, analysis of cycle timing on catalyst performance was feasible, and it was particularly developed in terms of constant overall amount of CO. This overall amount of CO could be defined as a function of parameter τ (Eqs. (2) and (3)).

$$\tau = \frac{t_L}{t_R} \tag{2}$$

$$n_{CO} = C_{CO} \cdot \frac{Q}{\tau} \tag{3}$$

All the reaction tests were performed at constant volumetric flow (Q) and constant CO concentration during rich periods (C_{CO}). Therefore, the overall amount of CO (CO molar flow, n_{CO}) was just dependent on the time lean-to-time rich ratio, τ. On the other hand, a back pressure control system was required in order to minimise pressure and flow changes upon switching on the solenoid valves.

The reactor was loaded with 3.2 g of the catalyst sample, which was located between two quartz beds. The top one allowed preheating of the gas mixture up to the reaction temperature whereas the lower one was used just as a support for the catalytic bed. The reactor tube was placed inside a 3-zone tube furnace, and the operating temperature was set at 350 °C for all the catalytic runs. Two thermocouples were placed at the top and bottom of the catalyst bed in order to record inlet and outlet gas temperatures.

Gas compositions at the reactor outlet were continuously measured using chemiluminescence (NO_x), flame ionization (C_3H_6), infrared (CO, CO_2, NH_3, N_2O, SO_2) and paramagnetic (O_2) detectors using Rosemount Analytical analysers. In order to verify the nominal inlet concentrations a bypass loop, which allowed the gas mixture to bypass the reactor, was used. Although it was not evaluated, H_2 formation from CO via water-gas-shift reaction during rich excursions should not be neglected. In order to quantify its eventual contribution, the WGS reaction was separately analysed in absence of NO_x and O_2 (2.0% CO, 8.4% H_2O, 8.4% CO_2, balance in N_2 with a flow rate of 4 N l min^{-1}). At 350 °C, the conversion at a steady state almost reached 40%. Note that its actual contribution under NSR operation conditions would be limited by the occurrence of competing parallel reactions, i–v [26], but in any case this reaction could not be ignored. NO_x conversion was established by time integration of the curves obtained during the transient storage-reduction experiments and subsequent application of Eq. (4).

$$NO_{x\,\text{Conversion}} = 100 \times \frac{[NO_x]_{in} - [NO_x]_{out}}{[NO_x]_{in}} = 100 \times \frac{[NO_x]_{in} - \int C_{NO_x}(t)dt}{[NO_x]_{in}} \tag{4}$$

Furthermore, the CO slip was also evaluated by time integration of CO concentration profiles during the runs and subsequent application of Eq. (5).

$$CO_{\text{Unconverted}} = 100 \times \frac{[CO]_{out}}{[CO]_{in}} = 100 \times \frac{\int C_{CO}(t)dt}{[CO]_{in}} \tag{5}$$

2.3. CO availability tests

Transient runs conducted in absence of NO_x and H_2O over a fully regenerated catalyst were also performed (lean conditions: 5% O_2, 8% CO_2, N_2 balanced, and rich conditions: 2% CO, 8.4% CO_2, N_2 balanced). CO outlet concentrations were measured during a series of transitions for different t_R values up to 50 s. This allowed the evaluation of the amount of CO (also valid for H_2 if WGS occurred by H_2O admission) that did not react with O_2 during the rich events. This amount was defined as CO availability and calculated using Eq. (5).

Gas-phase O_2 depletion by CO has been reported to be efficient over model NSR catalysts (in the studied temperature range) and it mainly takes place over a very small portion of the front of the catalyst [21]. Then, it is feasible to assume that this CO availability is an indirect measurement of the remaining CO that can play a role in adsorption site regeneration and subsequent NO_x reduction.

2.4. Real-flow characterisation

A series of stimulus–response tests were performed with the aim of describing the real-flow scenario during rich-to-lean and lean-to-rich transitions. O_2 was employed as a tracer and step stimulus-signals between 3% and 6% (minimising the possible contribution of O_2 storage effect) were applied using the SV2. O_2 concentration was monitored at two points which defined the test section: at the MP (1) and just at the reactor outlet (2). A Testo 350-XL portable analyser was employed on this task, since its relatively short mean residence time (~4 s) made it especially suitable for this kind of test. Anyway, on the basis of the described test conditions, mean residence times ($\bar{t}$) and variances of the concentration–time curves ($\Delta\sigma^2$) can be considered as additive [27]. This technique allowed any type of imperfect pulse to be employed and also compensated for the contribution of the analyser [28], thus, for the test section the following equations can be written as

$$\bar{t} = \bar{t}_2 - \bar{t}_1 \tag{6}$$

where mean residence time at location i can be calculated by Eq. (7) for evenly spaced time increments

$$\bar{t}_i = \frac{\sum_{t=0}^{t=\infty} t_i \Delta C_t}{\sum_{t=0}^{t=\infty} \Delta C_t} \tag{7}$$

and

$$\Delta\sigma^2 = \sigma_2^2 - \sigma_1^2 \tag{8}$$

where variances at location i can be calculated by Eq. (9) for evenly spaced time increments

$$\Delta\sigma_i^2 = \frac{\sum_{t=0}^{t=\infty} t_i^2 \Delta C_t}{\sum_{t=0}^{t=\infty} \Delta C_t} - \bar{t}^2 \tag{9}$$

Subsequent application of Eq. (10) resulted in calculating the axial dispersion modulus (δ_L/uL), which is characteristic of the flow behaviour (deviation from ideal plug flow) along the test section.

$$\frac{\Delta\sigma^2}{(\bar{t}^*)^2} = \frac{2\delta_L}{uL} + 8\left(\frac{\delta_L}{uL}\right)^2 \quad (10)$$

By means of a modification of the Fick's law [28], considering that SV1 and SV2 provided ideal discrete step changes in compounds concentrations, it was possible to estimate the concentration profiles of the different compounds at the reactor outlet, Eq. (11).

$$\frac{C - C_0^-}{C_0^+ - C_0^-} = \frac{1}{2}\left\{1 - erf\left[\frac{1}{2}\sqrt{\frac{uL}{\delta_L}}\left(\frac{1 - t/\bar{t}^*}{\sqrt{t/\bar{t}^*}}\right)\right]\right\} \quad (11)$$

where C_0^- and C_0^+ are the nominal concentrations before and after SV performance, respectively; *erf* is the error function which is tabulated in most handbooks of mathematical tables; and $\bar{t}^* = u/L$. For our particular reactor configuration, volumetric calculations indicated that the contribution to the residence time of the portion in between catalyst bed inlet and reactor outlet was only 5%. Therefore, it was assumed that those profiles could be also representative of those generated at the catalyst bed inlet.

3. Results and discussion

Reaction tests were performed at 350 °C and the obtained concentration and temperature profiles were recorded once stable performance was achieved after several cycle sets. This allowed continuous monitoring and therefore the determination of concentration and temperature profiles. Fig. 2 shows that the catalyst stored a considerable amount of NO_x clearly evidenced by the low NO_x outlet concentration during the first 150 s of the lean-stage. Afterwards, the continuous increase in the amount of NO_x going through the catalyst was assigned to the approximation to active adsorption sites saturation. During the rich periods the CO oxidation process seemed very efficient, since this component was only detected at the last stage of this period and when relatively high t_R (>20 s) were imposed. As a consequence, large amounts of CO_2 were generated. On the other hand, only trace amounts of N_2O were evolved at the beginning of this stage, which gradually decreased together with the NO_x concentration, while NH_3 formation was not observed.

Associated with the rich periods, a temperature rise was noticed at both the inlet and outlet of the catalyst bed. The exothermic contribution of CO–O_2 reaction during these rich periods has already been addressed [26]. Moreover, even when no O_2 is present in the gas composition of the regeneration phase, the contribution of the oxygen surface species, associated with the specific OSC component (probably ceria) in the commercial NSR catalyst investigated by these authors, can lead to large temperature increases when switching to a rich atmosphere [23]. However, since O_2 was not admitted during the rich events and our catalyst did not have a OSC phase, suggesting an additional cause for this exothermic event, different from those previously cited.

3.1. Effects of cycle timing on the catalyst performance

The control of time in the "*on mode*" of the solenoid valves allowed the analysis of the effect of cycle timing on catalyst performance. A set of 20 storage-reduction runs were performed at 350 °C for varying cycle timings, including five different values for t_R and/or four different values for τ parameter (Table 2).

Firstly, the integrated NO_x conversion is presented as a function of cycle length ($t_L + t_R$) in Fig. 3a. As expected, results clearly indicated that NO_x conversion efficiency strongly depended on τ

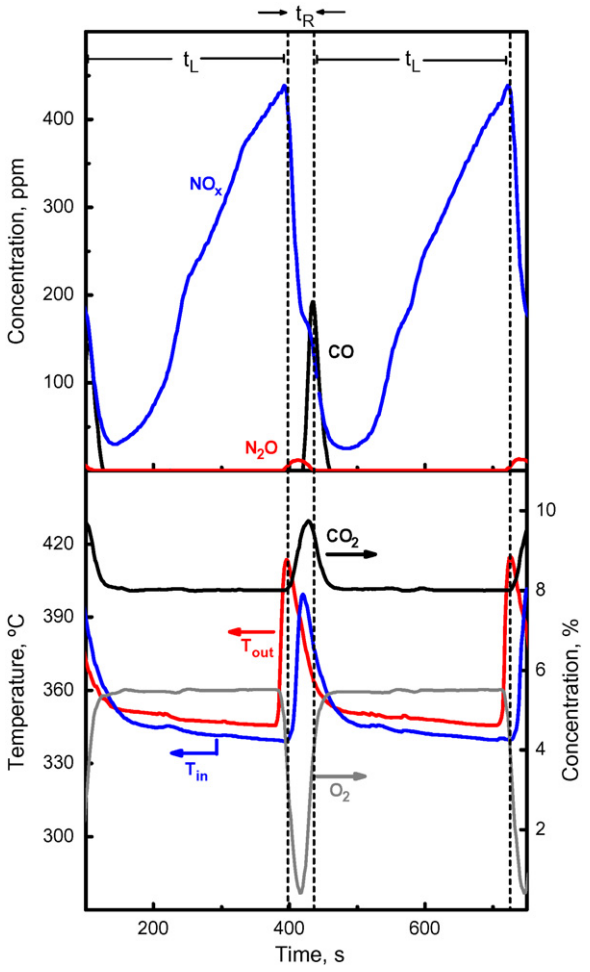

Fig. 2. Temperature and outlet concentration profiles for t_R/t_L = 30/300 s/s cycle test. Gas compositions are listed in Table 1. Dashed lines are indicative of the regeneration period.

Table 2
Experimental cycle timing levels.

Factor	Levels				
τ	4	7	10	14	
t_R, s	5	10	20	30	50

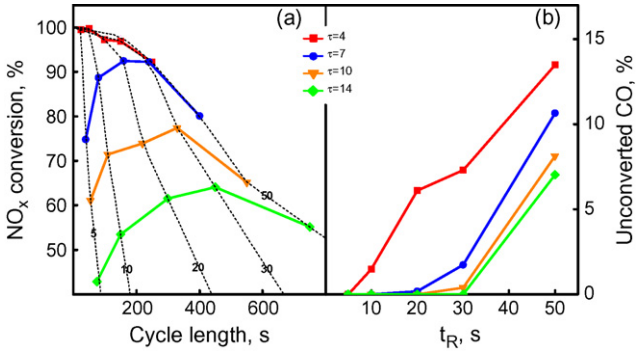

Fig. 3. NO_x abatement efficiency (a) and wasted CO amount (b) as a function of cycle timing. Dashed lines (a) are indicative of operation for constant t_R. Red, blue, orange and green lines correspond to operation with τ = 4, 7, 10 and 14, respectively. (For interpretation of the references to color in the figure caption, the reader is referred to the web version of the article.)

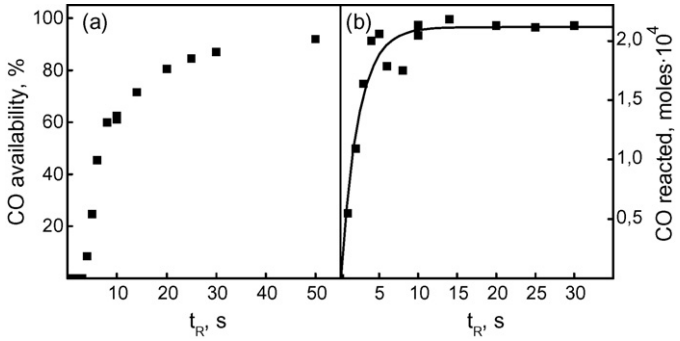

Fig. 4. Results from CO availability tests: dependences on t_R at 350 °C of the CO–O_2 availability (a) and the amount of CO per cycle involved in the reaction with oxygen (b).

parameter, and subsequently on the overall reductant amount. The increase in this ratio, for a given t_R (dashed lines), led to a reaction scheme closer to catalyst saturation, and the continuous increase in the amount of NO_x escaping the catalyst during the lean stages resulted in a global decrease of NO_x abatement efficiency. In agreement with the results found when simulating fuel injection (no O_2 suppression during rich periods) [24,25], for a given overall reductant amount (iso-τ lines), an optimum intermediate value for highest NO_x conversion could be determined for a specific cycle length. Over the studied operational conditions this optimum timing was achieved for t_R values ranging from 20 to 30 s. Excessively short cycle lengths resulted in a strong drop of NO_x conversion. On the other hand, for longer cycle lengths, the catalytic system tended again to operate closer to saturation during lean periods leading to poorer integrated NO_x conversions.

The amount of unconverted CO was also evaluated for this set of experiments by application of Eq. (5) (Fig. 3b). For $\tau = 4$, in spite of the dependence on t_R, it was evident that a large excess of reductant was used. Then, high NO_x conversions were achieved at the expense of a large amount of unconverted CO. The increase in τ parameter (equivalent to an increase in t_L for a given t_R) obviously corresponded to a reduction of the unconverted CO, leading almost to a complete removal of this compound at the outlet just for $\tau = 7$ and $t_R = 20$ s. Under these operational conditions the catalytic system still provided high NO_x conversions (up to 92%).

Anyway, it could be concluded then that the reaction system would operate with reductant defect for $\tau > 7$ and $t_R < 20$ s. The trends shown in Fig. 3b revealed that this defect would be marked with further τ increase and/or further t_R decrease. Under these CO defect operation conditions, NO_x conversion would be obviously limited by the regeneration-reduction step. Then the observed trends were related to NO_x conversion decay with τ increase (decrease in the overall amount of reductant). It could be also associated with the observed NO_x conversion decay with cycle length (at relatively low cycle lengths) for a given overall amount of reductant (constant τ). However, an incoherence arises from this last finding, since in a first consideration (if changes in the contribution of reaction i with cycle length is not considered), the amount of unconverted CO should be dependent just on the NO_x conversion when operation was maintained at constant τ. Furthermore, if the contribution of reaction i was not considered it could be expected that the amount of unconverted CO could be determined by just considering the stoichiometric coefficients of reactions ii–v. Therefore, it seemed that there was a noticeable contribution of CO–O_2 reaction which increased for shorter cycle lengths.

In order to analyse the relevance of this CO–O_2 reaction, a series of CO availability tests consisting of lean-rich transient runs in absence of H_2O and NO_x as described in detail in Section 2.3, was performed at 350 °C as a function of t_R (Fig. 4a). It was observed that CO availability strongly depended on t_R, especially for low t_R values. Within the $t_R < 20$ s range, additional reductions of this parameter promoted notable decays for CO availability, leading to total CO depletion for $t_R < 3$ s. This was in good agreement with both NO_x conversion (Fig. 3a) and unconverted CO amount decays (Fig. 3b) with cycle length reduction. In particular, NO_x conversion efficiency showed a marked worsening for very short t_R values (when shifting from 10 to 5 s) consistent with a strong decay in CO availability with t_R.

Since there was no specific OSC on the catalyst formulation, only two possible sources of oxygen could play a role in the CO–O_2 reaction. The first one was that at 350 °C Pt sites were likely to be covered by adsorbed oxygen (O_{ads}) at the end of each lean period [29]. Platinum oxides formation was neglected since it would require very long lean period times [30]. The contribution of this source of oxygen, in terms of the moles of oxygen adsorbed (n_{O-Pt}), was then estimated by the following equation:

$$n_{O-Pt} = \frac{m_C \cdot G \cdot D}{M_{Pt}} \cdot \gamma \quad (12)$$

where m_C is the amount of catalyst loaded in the reactor (g), G is the Pt content of the catalyst ($g_{Pt}\,g^{-1}$), D is the Pt dispersion ($g_{PtS}\,g_{Pt}^{-1}$), M_{Pt} is the molecular weight of Pt ($g_{Pt}\,mol_{Pt}^{-1}$) and γ is the O/Pt chemisorption ratio ($mol_O\,mol_{Pt}^{-1}$). Thus, assuming full coverage of Pt sites by chemisorbed oxygen with a ratio O/Pt = 1 [30,31], it was possible to estimate both the moles of atomic oxygen adsorbed at the end of the lean stage and subsequently, due to the reaction stoichiometry 1:1, the amount of CO that could be oxidised per cycle. This source accounted just for 6.6×10^{-6} mol of O_{ads} and of CO reacted per cycle.

Fig. 4b shows the amount of CO involved in the oxidation process per cycle. For low t_R (<3 s) the depletion of CO was complete and consequently the amount of CO reacted per cycle increased linearly. This increase was less noticeable for higher t_R values, reaching a plateau at 2.2×10^{-4} mol of CO per cycle. As can be deduced from Fig. 4b O_{ads} on Pt sites was not enough to account for the observed extent of the CO–O_2 reaction, contributing approximately to only 3% of the reacted CO per cycle.

On the other hand, analysis of the O_2 step stimulus signals and subsequent calculus of $\bar{t}$ and $\Delta\sigma^2$ (equal to 5.6 s and 2.2 s^2, respectively) by Eqs. (6)–(9), resulted in an axial dispersion modulus (δ_L/uL) equal to 0.03, which was representative of a relatively high mixing degree upstream from the catalytic bed. The time-dependant O_2 and CO composition profiles at the catalyst bed inlet, solid lines in Fig. 5, resulting from a discrete lean-to-rich transition could be then estimated by introducing this modulus into the Fick's law (Eq. (11)). For comparison composition profiles expected for ideal plug flow behaviour are also represented, dashed lines, considering a residence time of 5.6 s. Moreover, supposing that this CO–O_2 reaction took place over a negligible portion of the catalyst at the bed front and considering the 2:1 stoichiometry, the evolution of the CO available for NO_x release-reduction could be also estimated as shown also in Fig. 5.

According to the estimated composition profiles, one of those discrete transitions could correspond to 1.25×10^{-4} mol of CO reacted, so a maximum of 2.50×10^{-4} mol per cycle could be involved on reaction i due to the mixing effects. This source could then account for the experimentally observed CO conversions for high t_R values, of approximately 2.2×10^{-4} mol per cycle. This result is in concordance with that of Kabin et al. [25] who showed, for rich spikes promoted by fuel injection, a performance consistent with that of a mixed feed when excessively low cycle lengths were applied.

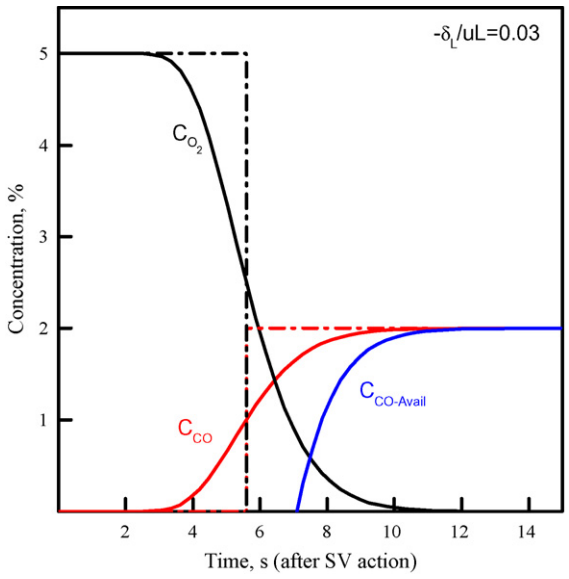

Fig. 5. Estimated O_2, CO and available CO concentration profiles at the catalyst bed inlet for a discrete lean-to-rich transition.

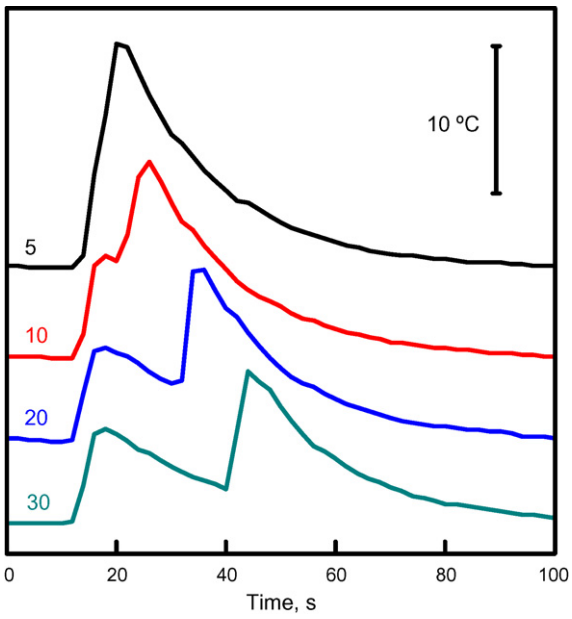

Fig. 7. Temperature profiles measured at catalyst bed inlet in absence of H_2O and NO_x for t_R of 5, 10, 20 and 30 s. The nominal temperatures were 349 and 340 °C at the catalyst bed inlet and outlet, respectively.

3.2. Effects of cycle timing on the distribution of the exothermic reactions

Fig. 6 shows the temperature profiles recorded during the performed storage-reduction runs under the nominal conditions for different cycle timings. The thermocouples in flowing N_2, indicated 349 and 340 °C constant values at the bed inlet and outlet, respectively. Upon switching under the storage-reduction run conditions, cyclic transient temperature responses were observed with a mean value increase in both locations. The sensors indicated higher temperature peaks in the inlet position with regard to the outlet one, as well as a time delay in between both maxima values. These trends in temperature were noted for each cycle timing. Anyway, modification of the cycle timing promoted changes in this cyclic transient temperature as shown in Fig. 6a–c. Qualitatively, when 10/20 s rich/lean cycle runs were conducted a quasi-sinusoidal response was observed at the inlet point. Meanwhile, the temperature at the outlet exhibited quite stable values. An increase in the mean temperature (ΔT^*) of almost 30 and 20 °C with regard to the nominal ones was observed at the inlet and outlet locations, respectively.

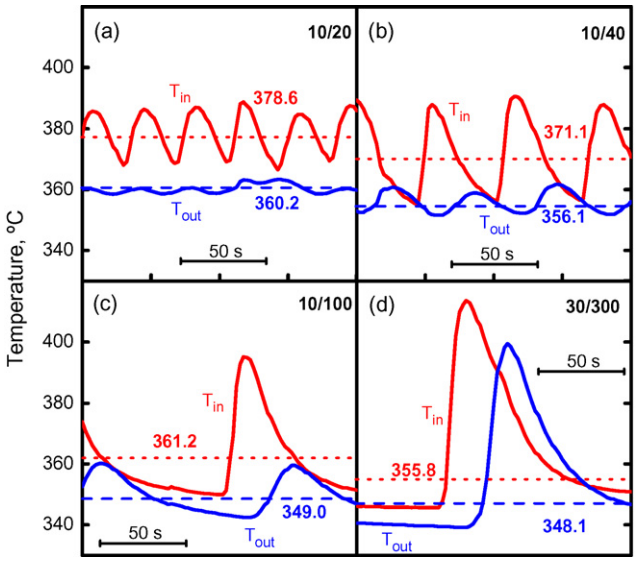

Fig. 6. Temperature profiles measured at catalyst bed inlet (red lines) and outlet (blue lines) for t_R/t_L (s/s) conditions of 10/20 (a), 10/40 (b), 10/100 (c) and 30/300 (d). Averaged temperatures are also shown for each case.

Longer lean periods, cases of 40 and 100 s are shown in Fig. 6b and c, resulted in discrete temperature increases showing sharper profiles, at the inlet location particularly, associated with the rich events. Meanwhile, ΔT^* values decreased towards zero. It could be also observed that long lean periods were required for the recovery of the reference values of temperature, indicative of a slow heat dissipation phenomenon. In contrast, no dependence was induced on the observed 26 s delay between the inlet and outlet maximum temperatures. On a basis of constant τ, the effect of cycle length modification was also analysed. The temperature profiles showed in Fig. 6d were recorded during 30/300 s rich/lean cycle runs. Sharper temperature profiles, particularly for the outer location, were evident compared with those obtained for 10/100 s rich/lean cycle runs. Again, no noticeable dependence was observed on the delay between the inlet and outlet maximum temperatures.

As previously indicated, the Ba/Pt–Al_2O_3 sample had no added OSC component, which may contribute to the heat delivery, and the target gas composition in the rich periods did not include any O_2. Then, the temperature profiles were associated with both O_2–CO mixing during lean-to-rich and rich-to-lean transitions and the heat generated by nitrites and nitrates reduction. On the other hand, the quasi-exponential increase of ΔT^* with decreasing τ (for a given t_R) could be interpreted in terms of both phenomena: NO_x conversion and O_2–CO mixing degree increase. It was safely assumed that the later effect was dominant since, as shown before, this O_2–CO mixing degree (dependent on the number of cycles per time unit) varies reciprocally with the cycle period. Meanwhile, NO_x conversion showed just a slight increase. A more accurate analysis of the contribution of NO_x reduction process to the exothermic events would require further considerations such as distinguishing between gas-phase NO_x and NO_x-ad-species reduction processes and even the nitrate-to-nitrite ratio reached at the regeneration onset [8].

Temperature profiles obtained over discrete rich events in absence of NO_x and H_2O in the feed stream are shown in Fig. 7. The contribution of the WGS reaction to the temperature profiles

was neglected due to the mildness of the own exothermic process [24]. The sharpness and morphology of the temperature increases notably differed from those obtained in the presence of NO_x (Fig. 6c and d). Then, the exothermic contribution of nitrite and nitrate reduction could not be neglected, especially when cycle length was relatively high. Under these conditions its contribution to ΔT^* could become dominant.

On the other hand, it could be assumed that the use of relatively low cycle lengths led to a NSR operation intensified over the catalyst front side, as the catalyst was oversized. Then, for constant τ, it should be expected that cycle length increase would extend the NSR operation axially through the catalyst. If the temperature profiles when switching from 10/100 to 30/300 s rich/lean cycles were compared, the aforementioned assumption would become evident, since in the later case both inlet and outlet temperature increases were of the same order. This behaviour could be explained just by a more axially extended NO_x ad-species reduction process, which intensified the heat release in the outlet position of the catalyst bed.

The scenario described by Epling et al. [23], where some heat is conductively transported on the axial direction through the catalyst at a lower rate than in the gas-phase, suitably explained the results since no notable change was observed in the delay between the inlet and outlet maximum temperatures for different t_R values. In the same way, model studies carried out by Sharma et al. [29] showed that thermal front generated at the inlet propagates along the reactor resulting in a maximum temperature at the reactor outlet well above in the lean phase. In our particular experimental device, this thermal front would take those 26 s to exit the reactor.

A further analysis of Fig. 7 showed that subtraction of the NO_x ad-species reduction contribution resulted in the presence of two exothermic events per cycle. This scheme was clarified when increasing t_R, allowing a certain advance of the heat dissipation process in between both lean-to-rich and rich-to-lean transitions. This result corroborated the presence of a notable contribution of the $CO–O_2$ reaction that took place during both transitions.

The eventual contribution of oxygen adsorbed on Pt sites (or of OSC components if were present in the formulation) would be associated with just the first exothermic event, when reducing atmosphere was switched. Qualitatively the extents of the temperature profiles of both transitions were quite similar. This confirmed the previous calculations regarding the negligible contribution of the oxygen adsorbed on the catalyst, since its effect would lead to a major exothermic event during the lean-to-rich transition if compared to the rich-to-lean one.

4. Conclusions

This work was focused on identifying optimal lean-rich feed timing and understanding the results of NO_x storage and reduction process. Experimental study using CO as the reductant on a $Pt/Ba/Al_2O_3$ catalyst powder was conducted. Results regarding the mixing between rich and lean pulses and the subsequent effect on the reactor performance in terms of NO_x and CO conversions were presented.

For a given overall amount of CO (constant τ), it was possible to tune its supply in terms of rich-lean cycle length in order to maximise the NO_x abatement efficiency. Timing mismatch due to operation under excessively long cycles resulted in poor NO_x abatement efficiencies together with high unconverted CO amounts leaving the system. From this scheme, reducing the cycle length led to higher NO_x and CO conversions. In addition, by selecting the correct overall amount of CO, it was possible to maintain high NO_x conversions (~90%) while minimising CO slip.

The deviation from ideal plug flow limited this trend. Under real-flow conditions, and even for a catalyst with OSC-free formulations, reducing the cycle length resulted in an increasing contribution of mixing effects of the $CO–O_2$ reaction due to rich-to-lean and lean-to-rich transitions. Therefore, when the cycle length was reduced beyond a certain level, and in spite of the constant overall amount of CO, the decrease in the availability of CO for NO_x ad-species reduction led to operation states with CO deficiencies and subsequently to a poorer NO_x conversion efficiency.

Obviously, the intensity of this effect due to the deviation from ideal plug flow will depend not only on the number of transition per time unit but also on the particular flow behaviour of each reaction scheme. Particularly, the need to operate under relatively short t_R (to minimise fuel penalty) in a real automotive application could magnify this effect. In addition, reducing cycle length, as a strategy to minimise the effect of deactivation processes (i.e., SO_2 uptake) on catalyst behaviour or to enhance catalytic converter performance at low temperatures, will be also limited by the real-flow conditions.

In any case, the need for a quantitative examination of the deviations from idealised flow behaviour seemed evident for the NSR catalyst performance comparison under realistic operational conditions and for the development of more representative models. In a first attempt, a simple model has been constructed that estimates concentration profiles originated from a discrete transition. This topic is the subject of our current research and will be reported elsewhere. Ongoing studies include tests with lab-made NSR monolith, and the extension of the aforementioned model to non-discrete transitions with the inclusion of gas-phase O_2 during rich periods.

Acknowledgments

The authors wish to thank Departamento de Educación, Universidades e Investigación del Gobierno Vasco (BFI05.258), Diputación Foral de Bizkaia (DIPE07/11), and Ministerio de Ciencia y Tecnología (CTQ2006-15079) for their financial support.

References

[1] R.J. Farrauto, R.M. Heck, Environmental catalysis into the 21st century, Catal. Today 55 (2000) 179–187.
[2] S. Matsumoto, Recent advances in automobile exhaust catalysts, Catal. Today 90 (2004) 183–190.
[3] Z. Liu, S.I. Woo, Recent advances in catalytic $DeNO_x$ science and technology, Catal. Rev. 48 (2006) 43–89.
[4] N. Miyoshi, S. Matsumoto, K. Katoh, T. Tanaka, J. Harada, N. Takahashi, K. Yolota, M. Sugiura, K. Kasahara, Development of new concept three-way catalyst for automotive lean-burn engines, SAE Tech. Pap. 950809 (1995) 121–130.
[5] W.S. Epling, L.E. Campbell, A. Yezerets, N.W. Currier, J.E. Parks, Overview of the fundamental reactions and degradation mechanisms of NO_x storage/reduction catalysts, Catal. Rev. 46 (2004) 163–245.
[6] K.S. Kabin, P. Khanna, R.L. Muncrief, V. Medhekar, M.P. Harold, Monolith, TAP reactor studies of NO_x storage on $Pt/BaO/Al_2O_3$: elucidating the mechanistic pathways and roles of Pt, Catal. Today 114 (2006) 72–85.
[7] D. James, E. Fourré, M. Ishii, M. Bowker, Catalytic decomposition/regeneration of $Pt/Ba(NO_3)_2$ catalysts: NO_x storage and reduction, Appl. Catal. B 45 (2003) 147–159.
[8] U. Elizundia, R. López-Fonseca, I. Landa, M.A. Gutiérrez-Ortiz, J.R. González-Velasco, FT-IR study of NO_x storage mechanism over $Pt/BaO/Al_2O_3$ catalysts. Effect of the Pt–BaO interaction, Top. Catal. 42–43 (2007) 37–41.
[9] L. Lietti, P. Forzatti, I. Nova, E. Tronconi, NO_x storage reduction over $Pt–Ba/\gamma$-Al_2O_3 catalyst, J. Catal. 204 (2001) 157–191.
[10] M. Piacentini, M. Maciejewski, A. Baiker, Pt–Ba/alumina NO_x storage-reduction catalysts: influence of Ba loading on NO_x storage behavior, Appl. Catal. B 60 (2005) 265–275.
[11] M.V. Twigg, Progress and future challenges in controlling automotive exhaust gas emissions, Appl. Catal. B 70 (2007) 2–15.
[12] K. Nakatani, S. Hirota, S. Takeshima, K. Itoh, T. Tanaka, K. Dohmae, Simultaneous PM and NO_x reduction system for diesel engines, SAE 2002 (2002-01-0957).
[13] W.S. Epling, D. Kisinger, C. Everest, NO_x storage/reduction catalyst performance with oxygen in the regeneration phase, Catal. Today 136 (2008) 156–163.
[14] C.M.L. Scholz, K.M. Nauta, M.H.J.M. de Croon, J.C. Schouten, Kinetic modelling of NO_x storage and reduction with different reducing agents (CO, H_2 and C_2H_4) on a $Pt–Ba/\gamma$-Al_2O_3 catalyst in the presence of CO_2 and H_2O, Chem. Eng. Sci. 63 (2006) 2843–2855.

[15] M.S. Brogan, R.J. Brisley, A.P. Walker, D.E. Webster, W. Boegner, N.P. Fekete, M. Krämer, B. Krutzsch, D. Voigtländer, Evaluation of NO_x storage catalysts as an effective system for NO_x removal from the exhaust gas of leanburn gasoline engines, SAE Tech. Pap. 952490 (1995) 1–9.
[16] H. Abdulhamid, E. Fridell, M. Skoglundh, Influence of the type of reducing agent (H_2, CO, C_3H_6 and C_3H_8) on the reduction of stored NO_x in a $Pt/BaO/Al_2O_3$ model catalyst, Top. Catal. 30–31 (2004) 161–168.
[17] T. Szailer, J.H. Kwak, D.H. Kim, J.C. Hanson, C.H.F. Peden, J. Szanyi, Reduction of stored NO_x on Pt/Al_2O_3 and $Pt/BaO/Al_2O_3$ catalysts with H_2 and CO, J. Catal. 239 (2006) 51–64.
[18] M. Piacentini, M. Maciewski, A. Baiker, Pt–Ba/alumina NO_x storage-reduction catalyst: effect of Ba-loading on build-up, stability and reactivity of Ba-containing phases, Appl. Catal. B 59 (2005) 187–195.
[19] K. Vaezzadeh, C. Petit, V. Pitchon, A. Kiennemann, A new concept for the removal of NO_x from a lean exhaust gas using storage on $H_3PW_{12}O_{40}{\cdot}6H_2$, a very fast desorption and reduction over a TWC, Catal. Commun. 3 (2002) 179–183.
[20] A. Bergmann, R. Brück, S. Brandt, M. Deeba, Design criteria of catalyst substrates for NO_x adsorber function, SAE Int. (2000) 159–164 (2000-01-0504).
[21] J.S. Choi, W.P. Partridge, C.S. Daw, Spatially resolved in situ measurements of transient species breakthrough during cyclic, low-temperature regeneration of a monolithic $Pt/K/Al_2O_3$ NO_x storage-reduction catalyst, Appl. Catal. A. 293 (2005) 24–40.
[22] W.S. Epling, A. Yezerets, N.W. Currier, The effects of regeneration conditions on NO_x and NH_3 release from NO_x storage/reduction catalysts, Appl. Catal. B 74 (2007) 117–129.
[23] W.S. Epling, A. Yezerets, N.W. Currier, The effect of exothermic reactions during regeneration on the NO_x trapping efficiency of a NO_x storage/reduction catalyst, Catal. Lett. 110 (2006) 143–148.
[24] R.L. Muncrief, K.S. Kabin, M.P. Harold, NO_x storage and reduction with propylene on Pt/BaO/alumina, AIChE J. 50 (2004) 2526–2540.
[25] K.S. Kabin, R.L. Muncrief, M.P. Harold, NO_x storage and reduction on a Pt/BaO/alumina monolithic storage catalyst, Catal. Today 96 (2004) 79–89.
[26] J.S. Choi, W.P. Partridge, W.S. Epling, N.W. Currier, T.M. Yonushonis, Intra-channel evolution of carbon monoxide and its implication on the regeneration of a monolithic $Pt/K/Al_2O_3$ NO_x storage-reduction catalyst, Catal. Today 114 (2006) 102–111.
[27] K.B. Bischoff, O. Levenspiel, Fluid dispersion-generalization and comparison of mathematical models. I. Generalization of models, Chem. Eng. Sci. 17 (1962) 257–264.
[28] C.G. Hill, Deviations from ideal flow conditions, in: C.G. Hill (Ed.), An Introduction to Chemical Engineering Kinetics and Reactor Design, John Wiley & Sons, New York, 1977, pp. 388–424.
[29] M. Sharma, M.P. Harold, V. Balakotaiah, Analysis of periodic storage and reduction of NO_x in catalytic monoliths, Ind. Eng. Chem. Res. 44 (2005) 6264–6277.
[30] L. Olsson, E. Fridell, The influence of Pt oxide formation and Pt dispersion on the reactions $NO_2 \leftrightarrow NO + (1/2)O_2$ over Pt/Al_2O_3 and $Pt/BaO/Al_2O_3$, J. Catal. 210 (2002) 340–353.
[31] A. Bourane, D. Bianchi, Oxidation of CO on a Pt/Al_2O_3 catalyst: from the surface elementary steps to lighting-off tests, J. Catal. 209 (2002) 114–125.